

The Physiological Underpinnings of Visual Short-Term Memory Binding using Graph Modular Dirichlet Energy: Evidence from Healthy Subjects

Keith Smith^{1,2,*}, Benjamin Ricaud³, Nauman Shahid³, Stephen Rhodes⁴, John M. Starr², Augustin Ibáñez^{5,6,7,8,9}, Mario A. Parra^{2,4,10,11,12}, Javier Escudero¹, and Pierre Vanderghenst³

¹Institute for Digital Communications, University of Edinburgh, West Mains Rd, Edinburgh, EH9 3FB, UK

²Alzheimer Scotland Dementia Research Centre, University of Edinburgh, 7 George Square, Edinburgh, EH8 9JZ, UK

³Signal Processing Laboratory 2, École Polytechnique Fédérale de Lausanne, 1015 Lausanne, Switzerland

⁴Human Cognitive Neuroscience and Centre for Cognitive Ageing and Cognitive Epidemiology, Department of Psychology, University of Edinburgh, EH8 9JZ, UK

⁵Institute of Translational and Cognitive Neuroscience (INCyT), INECO Foundation, Favaloro University, Buenos Aires, Argentina

⁶National Scientific and Technical Research Council (CONICET), Buenos Aires, Argentina

⁷Universidad Autónoma del Caribe, Barranquilla, Colombia

⁸Department of Psychology, Universidad Adolfo Ibáñez, Santiago, Chile

⁹ARC Centre of Excellence in Cognition and its Disorders, Sydney, Australia

¹⁰Psychology Department, Heriot-Watt University, Edinburgh, EH14 4AS, UK

¹¹Universidad Autónoma del Caribe, Barranquilla, Colombia

¹²UDP-INECO Foundation Core on Neuroscience (UIFCoN), Diego Portales University, Santiago, Chile

*k.smith@ed.ac.uk

ABSTRACT

Visual short-term memory binding tasks are a promising early biomarker for Alzheimer's disease (AD). To uncover the functional deficits of AD in these tasks it is necessary to first study unimpaired brain function. Electroencephalogram recordings were obtained from encoding and maintenance periods of tasks performed by healthy young volunteers. We probe the task's transient physiological underpinnings by contrasting shape only (Shape) and shape-colour binding (Bind) conditions, displayed in the left and right sides of the screen, separately. Particularly, we introduce and implement a novel technique named Modular Dirichlet Energy (MDE) which allows robust and flexible analysis of the functional network with unprecedented temporal precision. We find that connectivity in the Bind condition is stronger than in the Shape condition in both occipital and frontal network modules during the encoding period of the right screen condition. Using MDE we are able to discern driving effects in the occipital module between 100-140ms, which coincides with the P100 visually evoked potential, and a driving effect in the interaction of occipital and frontal modules between 120-140ms, suggesting a delayed information processing difference between these modules. This provides temporally precise information over a heterogeneous population for tasks showing promise in the detection of AD.

Introduction

Visual Short-Term Memory (VSTM) tasks prove promising in the early detection of Alzheimer's Disease (AD). A useful paradigm lies in tasks which are specifically designed to test the ability of participants to store information of either shapes alone (Shape) or shapes with associated colours (Bind) for short-term memory recognition. In this instance it is found that patients are particularly impaired in the Bind condition^{1,2,3}. This VSTM task has been found to be both sensitive and specific to early AD³ making it promising in the detection of preclinical disease^{1,2,4}. Our understanding of brain function relating to these tasks is incomplete due to technical limitations in analysis of brain recordings and neuroscientific limitations in understanding. It is clear that overcoming the former can guide the advancement of the latter. Thus, we set out to apply a novel signal processing approach to healthy brain functioning in order to uncover unimpaired brain processes which can help to guide future studies in the clinical setting. To this end, we contrast Shape and Bind conditions across healthy young subjects wearing

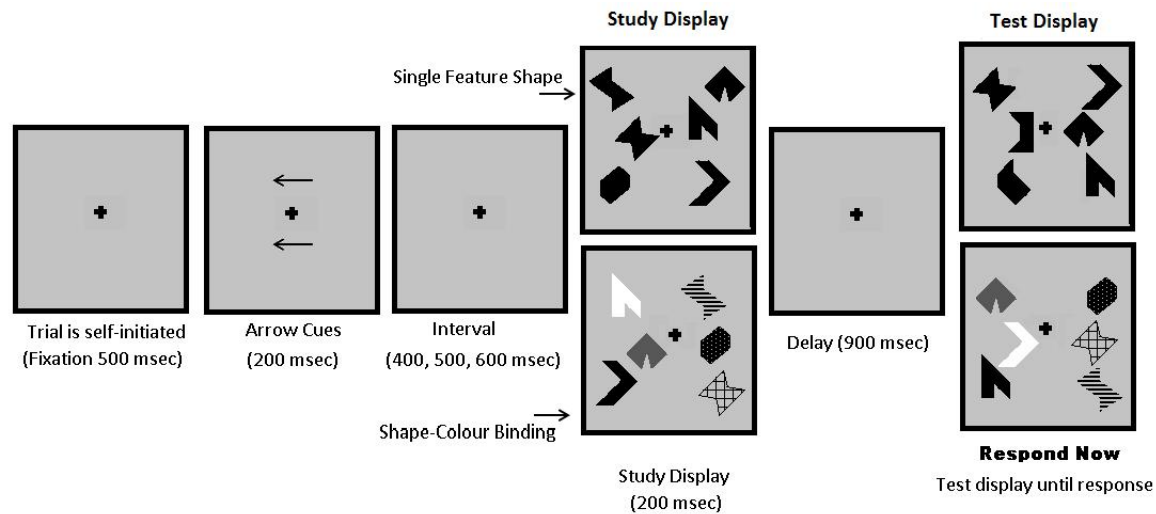


Figure 1. Chronology and design of the Visual Short Term Memory tasks. Arrow cues indicate to the participant the hemisfield being tested before stimulus.

an Electroencephalogram (EEG) to probe working memory integrative function at a high temporal resolution. In this study, we look at a set of VSTM cognitive tasks distinguished by two sets of binary conditions- Shape or Bind objects displayed in the left or right side of the screen (hemisfield), performed by healthy young volunteers, see Fig. 1. The Shape or Bind conditions allows the probing of the working memory integrative function whilst the hemisfield condition allows the exploration of contralateral sensitivities in brain activity to task performance.

The evidence gathered to date with the VSTM binding test comes from behavioural^{1,2,3,5} and neuroimaging studies⁶. Only one study has used EEG to investigate the early impact of AD on the mechanisms supporting this memory function⁷. None of these studies have addressed the issue of network organization and brain connectivity as the likely mechanisms sub-serving this memory function in intact brains. Should the brain network approach developed here prove informative with regard to unimpaired binding functions carried out in VSTM, this will create new opportunities to further investigate the impact of AD on memory. This is particularly relevant if we consider that AD causes severe brain disconnection from its very early stages^{8,9}.

Several studies^{5,10,11} have demonstrated that there is no impairment in VSTM task performance due to healthy ageing so we do not expect the functionality of the brain to be different in these tasks for healthy old people and healthy young people. Thus, the information provided in this study should not pose age-translational problems to future research in the clinical setting.

EEG recordings provide a unique opportunity to deepen our understanding of human brain function across a healthy lifespan and in diseases of the nervous system¹². In the clinical context, the low cost and portability of the EEG offers a strong feasibility for screening purposes. Pertinently, it can aid in the early detection of brain dysfunction associated to diseases which have an impact on the worldwide population, such as dementia^{13,14,15}. In a broader context, the high temporal resolution of the EEG presents a great opportunity to study the rapid interdependent processes which underlie cognition¹². Thus, the EEG provides an unparalleled matching of practicality and data richness for neurological diagnostics.

In order to analyse the EEG recordings of these cognitive tasks, which generally require dynamic interactions between different brain areas, we focus on functional networks¹⁶. Functional networks derive from network science which is a broadly applicable framework for understanding systems of interdependently acting agents. It is increasingly used in studies of brain function where bivariate connectivity methods applied to pairs of channels permits the construction of graphs which, in turn, leads to the identification of functional networks^{17,18,19}. Such an approach is unveiling the functional architecture of the human brain, helping us to understand its vulnerability to brain diseases^{16,20}. In our setting, each node of the graph corresponds to an electrode placed on the scalp and the connection strength is the correlation of the time-series recorded at the electrodes. Because EEG channels pick up weak electromagnetic activity propagated through many layers of tissue and bone, the reproducibility of EEG activity over a heterogeneous population is difficult to ascertain. To address this, we choose to analyse modules of the network defined by several channels placed over localised spatial regions of the scalp. In this way the exact placements of EEG channels with respect to the underlying subject physiology becomes less relevant and so by focusing on these modules we expect a better sensitivity to consistent effects over many subjects.

Exploiting the temporal resolution of EEG recordings in functional brain networks is an open problem ripe for exploration which, importantly, requires theoretical solutions and advancements^{21,22,23}. Because the reliability of connectivity information

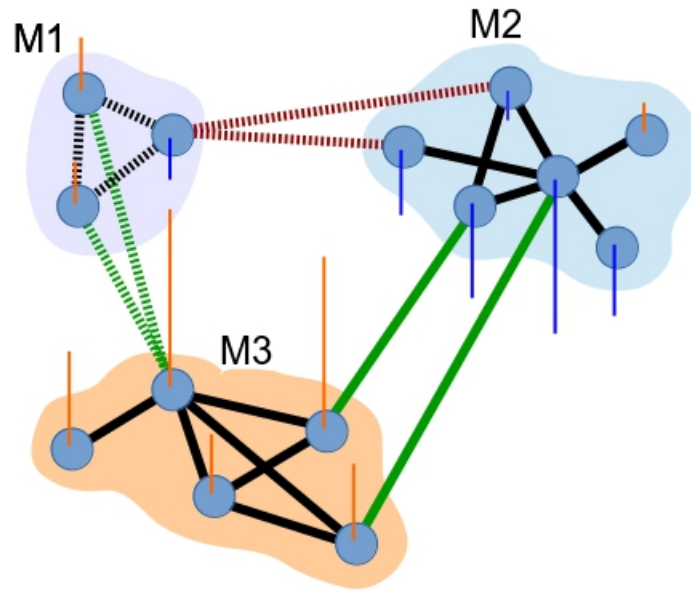


Figure 2. Illustration of a graph with a graph signal, indicated by the orange (positive) and blue (negative) lines at the nodes, decomposed into modules M1, M2 and M3. The dashed lines indicate all the edges associated with module M1.

is dependent on the number of time samples used, constructing networks over very short time epochs is implausible, which has heretofore restricted the ability to study rapid functional dynamics. To overcome this problem we introduce Modular Dirichlet Energy (MDE), a novel methodology based on graph signal processing²⁴.

Graph signal processing is a new theoretical branch which combines graph theory and signal processing^{24,25}. In this setup, each node is intrinsically associated with some measurement or value regarded as a sample of a graph signal. This signal is not temporal but topological, so that the graph edges correspond to the topology over which the signal is supported²⁴. Some evident applications of this field include the ability to filter a set of signals over a suitable graph topology, i.e. topological or spatial smoothing, or to use some measure of smoothness of the graph signal itself for hypothesis testing. The applicability of such methodology to the EEG is obvious since, during its recording, numerous channels are simultaneously sampled over the scalp. We take the graph signal as the EEG recording at each electrode, hence a time-series is associated to each node.

To study graph signals for specific modules, we set out the theory for MDE which combines Dirichlet energy, a measure of variability for functions, as it relates to graph signal processing²⁴ with the concept of modules from network science²⁶. Essentially, because of the one-to-one mapping of the components of Dirichlet energy with the edges of the underlying graph, given a well defined theoretical construct, the Dirichlet energy can be decomposed into modules which can then be analysed separately and interactively over the network. This allows for localised hypothesis testing of the graph signal, in turn allowing elegantly for the analysis of the specified brain modules in our study at an unprecedented level of temporal precision for functional brain network analysis.

Based on recent fMRI⁶ and EEG studies^{7,27} we predict significant involvement of modules which map onto the functional network of working memory. Posterior regions (parietal-occipital) have been reported as important nodes of the network supporting VSTM binding tasks⁶. Additionally, Parra et al.²⁷ and Pietto et al.⁷ recently reported involvement of frontal regions previously unnoticed by fMRI but known to be relevant to binding functions carried out in working memory²⁸. These authors argued that due to the high temporal resolution of the EEG, transient brain activity occurring in short time windows may be better detected by electrophysiological rather than fMRI techniques. Regarding laterality Parra et al.²⁷ recently reported hemispheric asymmetries during the retrieval phase in EEG while another study⁶ showed left hemisphere lateralisation in fMRI. Our methodological approach thus aims to unveil the network organisation that underpins such discrepancies by analysing transient dynamics of frontal and occipital modules. Furthermore we hypothesise that these regional activities are parts of an interdependent functional process and so we predict a specific difference in the activity between these modules which we analyse with Between MDE (BMDE).

Methods

Our methodological approach contrasts network analysis of Shape and Bind conditions at two levels- modular weights of long-term task-related epochs and MDE of short-term windows. The first level uses a standard analysis of connectivity weights in order to discern which epochs (encoding and maintenance), conditions (Left and Right) and modules (Frontal and Occipital) reveal sensitive functional differences between Shape and Bind tasks. We then probe those discoveries for transient temporal dynamics by implementing the novel MDE analysis over 20ms windows. This ensures a rigorous process of discovery which can be easily replicated for other research questions.

Visual Short-Term Memory Tasks and Data Acquisition

Stimuli: The stimuli were non-nameable shapes and non-primary colours known to be difficult to rehearse verbally^{1,6}.

Procedure: Two arrays of three items each were presented to the left and to the right of a fixation cross centred on the screen on a grey background (Fig. 1)¹¹. Each array was presented in a virtual 3x3 grid, 4° horizontally and 8° vertically centred and 3° to the left and right from fixation. Each item held 1° and the distance between items was never less than 2°. Items for the study display were randomly selected from a set of eight polygons and eight colours¹ and randomly allocated to 3 of the 9 positions within the grid. At test the items randomly shuffled within the same locations used in the study display. Hence, items were never presented in the same locations across study and test displays. This rendered location uninformative.

Trials were self-initiated. A fixation cross appeared in the centre of the screen and remained on throughout the trial. After a button press, 500ms lapsed before the arrow clues were presented. Two arrows appeared for 200ms one above and one below fixation which indicated which of the two visual arrays (left or right) the participants were to attend. An interval of random duration selected from 400, 500 or 600ms followed the cues. The study display was then shown for 200ms. After an unfilled retention interval of 900 ms the test display appeared and remained visible until the participant responded.

In the Shape condition each array of the study display presented three black shapes. The test display also showed three shapes. In 50% of the trials the content of the test display matched the content of the study display (“same trial”). The test display for the “different trials” showed two new shapes. In the Bind condition each visual array consisted of three shapes in different colours. In the test display for the “different trials” two coloured shapes swapped their colours. The participants responded “same” or “different” by pressing two keys previously allocated with both hands. The participants completed 8 practice trials before undergoing 170 test trials for each of the conditions.

Each participant undertook four different conditions of the VSTM task which are distinguished by two different binary manipulations- $2^2 = 4$.

1. Shape or Bind: the test items consist of black shapes (shapes only) or shapes with colours (shape-colour binding).
2. Left or Right: the test items are shown on the left side or the right side of the screen (or hemisfield) to which the participant is prompted before stimulus onset.

The task was to detect whether or not a change occurred across two sequential arrays shown on an initial study display and a subsequent test display.

EEG signals were recorded for 23 healthy young volunteers while they performed these VSTM tasks. Five of the volunteers were left-handed and eight were women. The mean and standard deviation ($M \pm SD$) of the age of participants and number of years of education is 23.0 ± 4.3 and 17.1 ± 2.8 , respectively. Informed consent was obtained from all subjects. The study was approved by the Psychology Research Ethics Committee, University of Edinburgh, and methods in data collection were carried out in accordance with their guidelines.

The EEG data was collected using NeuroScan version 4.3. The EEG was sampled at 250 Hz. A bandpass filter of 0.01-40 Hz was used. Thirty EEG channels, corrected for ocular artefacts using ICA, were recorded relying on the 10/20 international system. Fig. 3 shows the electrodes used in the analysis.

Further artefact rejection was conducted, rejecting trials which contained magnitudes of voltage fluctuations above 200 microvolts, transients above 100 microvolts and electro-oculogram activity above 70 microvolts. Only the trials with correct responses were kept as incorrect responses do not inform on working memory load in task comparisons. It is important to emphasise the distinction between a study of healthy brain function of task performance, as conducted here, for which the number of correct trials is not indicative, and a study of the performance of tasks by healthy people, for which the number of correct trials is indicative. In a few cases, no useful data was available for a volunteer performing one of the conditions resulting in an unequal number of volunteers per condition.

To keep comparisons straightforward, we chose only to look at those 19 participants of the original 23 for whom data on all of the conditions was available. We focused on the encoding (i.e., study display) and maintenance (delay) periods of VSTM, since these seem to be the stages of memory informing about the functional principles of organisation with regard to capacity and format of representation (Shape vs Bind)⁶.

The mean \pm standard deviation over participants for the number of kept trials for each condition were as follows: Shape, Left hemisfield- 69.74 ± 6.67 ; Bind, Left hemisfield- 63.79 ± 8.72 ; Shape, Right hemisfield- 66.32 ± 15.06 ; Bind, Right hemisfield- 63.58 ± 16.26 .

Modular Dirichlet Energy

Let $G = (\mathcal{V}, \mathbf{f}, \mathcal{E}, \mathbf{W})$ be the mathematical representation of an undirected, labeled graph where $\mathcal{V} = \{1, \dots, n\}$ is the vertex set of the graph, $\mathbf{f} = \{f_1, f_2, \dots, f_n\}$ is the graph signal, or vertex amplitudes, indexed by \mathcal{V} , $\mathcal{E} = \{(i, j) \text{ s.t } i \text{ is adjacent to } j \text{ for } i, j \in \mathcal{V}\}$ is the edge set with $|\mathcal{E}| = 2m$ and

$$\mathbf{W} = \begin{cases} w_{ij} & (i, j) \in \mathcal{E} \\ 0 & \text{otherwise} \end{cases}$$

is the positive weighted adjacency matrix of edge weights indexed by \mathcal{E} , where w_{ij} is a measure of strength of relationship between nodes i and j . Then we call $(\mathcal{V}, \mathbf{f})$ the vertex space of the graph and $(\mathcal{E}, \mathbf{W})$ the edge space of the graph so that G is a dual space composed of the vertex and edge spaces where every element of the edge set in the edge space is an ordered pair of elements from the vertex set in the vertex space.

An example of a graph with a graph signal is shown in Fig. 6. The blue circles represent the nodes of the network and the lines connecting them represent the edges. The graph signal is composed of the node amplitudes which are represented in Fig. 6 by the orange and blue lines- positive and negative values, respectively. The full mathematical formulation of MDE and derivation of the formula for its computation is given in the supplementary material.

A module of a graph is defined by a subset of nodes and all adjacent edges to those nodes, i.e. $(\mathcal{V}_X, \mathcal{E}_X)$ where $\mathcal{V}_X \subset \mathcal{V}$ and $\mathcal{E}_X = \{(i, j) : i \in \mathcal{V}_X, j \in \mathcal{V}\}$.

Likewise, the modular weights constitute the set $\{w_{ij} : i \in \mathcal{V}_X, j \in \mathcal{V}\}$ and we define the total modular weight, $w_{\mathcal{V}_X}$, as

$$w_{\mathcal{V}_X} = \sum_{i \in \mathcal{V}_X} \sum_{j \in \mathcal{V}} w_{ij}, \quad (1)$$

for module \mathcal{V}_X . This allows us to probe the weighted connectivity information of the modules of relevant brain regions in the context of the whole network.

Now, the Dirichlet energy of the graph G is defined as

$$E(G) = \sum_{i,j=1}^n w_{ij}(f_i - f_j)^2, \quad (2)$$

which is an inverse measure of the smoothness of the graph signal \mathbf{f} over G^{24} . We see this since the largest terms in the sum constitute connections with a strong relationship but whose node amplitudes have a large difference. On the other hand, the smallest terms are connections with a weak relationship and whose node amplitudes have a small difference, which is ambiguous in meaning. Particularly, the node gradient at node i is an important measure of the smoothness of the graph signal at node i and is defined as

$$E(i) = \sum_j w_{ij}(f_i - f_j)^2. \quad (3)$$

Note that the elements in the sum of (6) have a one to one mapping to the edge set, \mathcal{E} , of G . It follows that there is a natural decomposition of the Dirichlet energy in (6), corresponding to any disjoint composition of the underlying graph into modules, such that

$$E(G) = \sum_{x=1}^M \sum_{i \in \mathcal{V}_x} \sum_{j \in \mathcal{V}} w_{ij}(f_i - f_j)^2,$$

and we define the Modular Dirichlet Energy (MDE) of \mathcal{G}_x to be

$$MDE(\mathcal{G}_x) = \sum_{i \in \mathcal{V}_x} \sum_{j \in \mathcal{V}} w_{ij}(f_i - f_j)^2. \quad (4)$$

The dashed lines in Fig. 6 represent all the edges, and corresponding Dirichlet energy components, of the module M1. Further, we can define the between module Dirichlet energy (BMDE) as

$$BMDE(\mathcal{G}_x, \mathcal{G}_y) = \sum_{i \in \mathcal{V}_x} \sum_{j \in \mathcal{V}_y} w_{ij}(f_i - f_j)^2, \quad (5)$$

for two disjoint modules \mathcal{G}_x and \mathcal{G}_y . In Fig. 6, the black lines represent within module edges and energy components of each module and the dashed brown lines indicate the between module edges and energy components of modules M1 and M2.

For graph signals which also have a temporal dimension, i.e. $\mathbf{F} = [\mathbf{f}^0, \mathbf{f}^1, \dots, \mathbf{f}^Y]$, an $n \times Y$ matrix of chronologically ordered graph signals $\mathbf{f}^i = \{f_1^i, f_2^i, \dots, f_n^i\}$, the Dirichlet energy of the signal during time period $[t_0, t]$ is just the sum of the individual Dirichlet energies at each point in time:

$$E(G)|_{[t_0, t]} = \sum_{s=t_0}^t \sum_{i,j=1}^n w_{ij}(f_i^s - f_j^s)^2.$$

Thanks to linearity, this extends straightforwardly to all definitions above. By looking at short intervals of graph signals, $[t_0, t]$, we can study moments in time of the network behaviour by looking at the graph signal in the short interval acting over the graph defined by connectivity of the whole epoch and thus probe the connectivity information for dynamic behaviour within the epoch on which the graphs are constructed.

MDE analyses temporal brain networks from a completely different angle to other state-of-the-art methods such as temporal networks²⁹ or time series analysis of network metrics³⁰. Rather than being based on the construction of different networks indexed by chronology, MDE constructs just one network of general connectivity patterns over a larger epoch and uses this network as the support for localised time-series analysis of shorter windows. The activity is encoded in the graph signal rather than in the edge weights of a time-varying graph. This thus allows the direct probing of given network for shorter epochs which is arguably more elegant and directly comparable for transient dynamics than probing relations of several different networks corresponding to staggered time windows. Further, MDE works on weighted networks, as are ubiquitously generated by functional connectivity analysis, as well as binary networks, whereas multi-layer network approaches are generally based on the “existence - non-existence” edge criteria of binary networks.

Given that the components of the total modular weight are exactly those weights corresponding to the MDE of a given module, that the MDE is dependent on the underlying long-term modular edge weights and that the windows chosen for MDE are arbitrary, we recommend a two-level analysis approach. In the first level the data is probed over a long-term window using total modular weights. In the second level analysis of short-term windows using MDE is implemented. We demonstrate this approach in this study.

Pre-processing and module selection

The 30 channels were re-referenced to the average EEG activity. From the continuous EEG, we extracted epochs of 1.2 seconds starting at -200ms pre-stimulus onset (baseline). These epochs contained activity associated with the encoding and maintenance periods of the VSTM tasks. To further remove artefacts, channels with activity of a mean amplitude greater than 30 μV (2 Standard Deviations -SD) were rejected. We then computed the average ERP signal over correct trials (number of correct trials per participants, per condition: mean- 65.7, SD- 9.27) for each VSTM condition performed by each participant resulting in a set of 4×19 thirty-channel EEG signals. We focused on activity in two time windows, one reflecting the encoding period (0-200ms) and one the maintenance period (200-1000ms). For each of the set of mean 30 channel signals, a graph was created for both time windows where the electrodes were mapped one to one with nodes and the edge weights were defined as the absolute value of correlation coefficient between the pairwise channels for the broadband of frequencies (0.01-40Hz). We also set the node amplitudes as the signals zero averaged over the channel space for each time sample.

In order to find differences in cognitive task conditions that are representative of the sampled population (e.g., controlling for sources of individual variability such as head size, small electrode displacements, etc.), we considered activity over broader regions involving several electrodes (mapping to modules in graph theory). To this aim, we defined two modules on the graphs using well known brain regions (see Fig. 3) which are relevant to working memory processing³¹ and previously reported to be involved in the task investigated^{6,32}. These are the frontal module (F3, Fz, F4, FC3, FCz & FC4) and the occipital module (O1, Oz, O2, PO1 & PO2). The composition of these modules (i.e., electrodes chosen) was refined by considering the node gradient (7) computed for each node of the graph during the entire encoding and maintenance period to determine their suitability for the modules (i.e., using energy to identify outliers). For instance, if we consider the suitability of electrodes FP1 and FP2 for the frontal module, we see these electrodes have node gradients over 2 standard deviations (SD) above the mean drawn from the entire electrode array (248.72 ± 74.14 mean \pm SD) and even more extreme when considering just the frontal module (see Table 1), thus we excluded them to avoid their overpowering influence. Normalisation to correct for such influences is neither obvious nor advisable since each edge in a graph corresponds to two nodes and any such process would act to negate the scale-free nature of the underlying EEG network topologies³³.

We investigated differences in the encoding period (0-200ms) and the maintenance period (200-1000ms) of the tasks by analysing the total modular weight, $w_{\gamma_x}(1)$, of the specified modules.

We contrast these values for Shape vs Bind conditions in the left hemisfield and in the right hemisfield using paired t -tests. Implementing the novel MDE (4) concepts, where the graph signal is implemented over a reduced number of samples within the

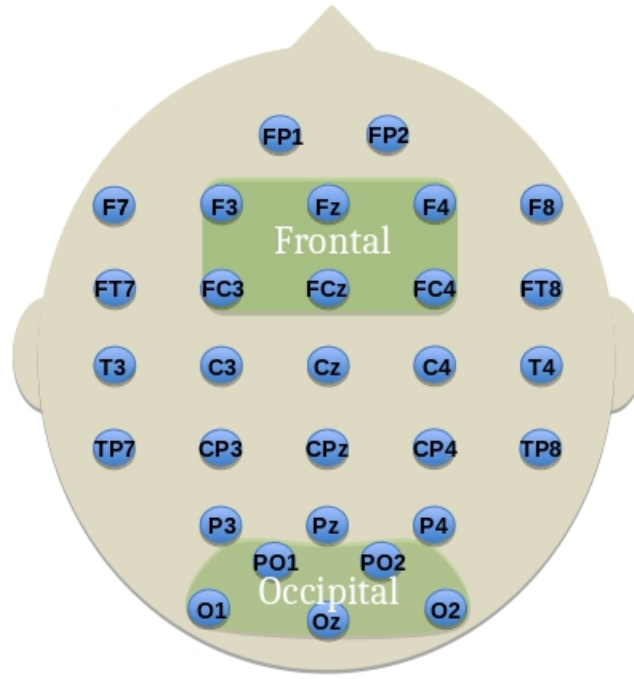


Figure 3. The frontal and occipital modules defined for network analysis. Labelled electrodes follow the 10-20 system.

epochs, we introduce a second level of analysis to discover if particular parts of the original epochs are driving the discovered effects. Given the clear hierarchical structure of the hypotheses, it is then necessary to use hierarchical False Discovery Rate (FDR)³⁴ to control for Type-I errors. Hierarchical FDR follows a level by level procedure of false discovery detection where a parent-child relationship is evident between these levels. Only those hypotheses whose parents were accepted as true discoveries are considered in the next level. In our study, the parent hypotheses relate to the total modular weights and the child hypotheses relate to the MDE analysis. Fig. 4 shows a model of a hypothesis hierarchy and the principles of rejection and acceptance of discovery through the FDR corrective procedure. We implemented a strict FDR with $q = 0.05$ throughout the procedure.³⁴

From the effects found in the edge weight testing, we compute the MDE for the frontal and occipital modules and the BMDE between the frontal and occipital modules. Note that $\text{BMDE}(\mathcal{G}_x, \mathcal{G}_y) \subset \text{MDE}(\mathcal{G}_x)$, so that we probe the modules specifically for the interaction of the frontal and occipital modules.

Results

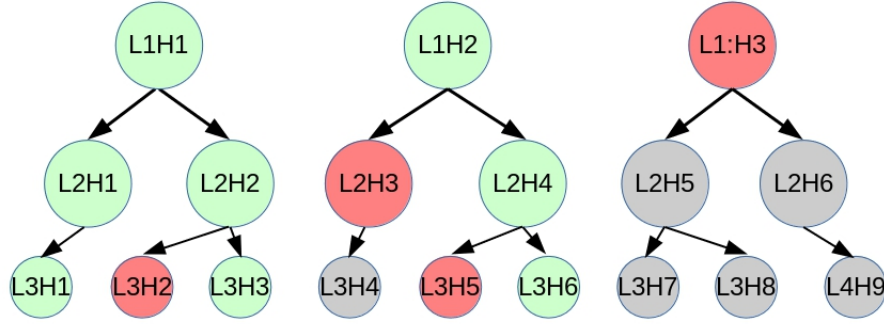
A summary of the results at two levels of analysis is presented in Tables 2 & 3. Paired t -tests were performed over participants for the measurements obtained for Shape and Bind conditions. The paired t -test is a one-sample t -test with mean 0 on the values $(X - Y)$ for paired observations X and Y across subjects. With respect to our study, X is a network metric of Bind task activity and Y of Shape task activity. Therefore the null hypothesis is that Shape and Bind values come from the same normal distribution, i.e. $\text{mean}(X - Y) = 0$. The alternative hypothesis is that Shape and Bind values come from normal distributions with different means, i.e. $\text{mean}(X - Y) \neq 0$. The normality of the distributions was tested for each paired t -test using the one-sample Kolmogorov-Smirnov test. No significant deviations from the normal distribution were found at the 5% level. Thus, the normality assumption underlying the paired t -tests is reasonable. The subsequent p -values were controlled using hierarchical FDR³⁴, allowing powerful probing of shorter time epochs of the discoveries found. We report the following:

Level 1

In the first level, the long-term total modular edge weights are analysed for the conditions to be contrasted. These contrast are Left Shape vs Left Bind and Right Shape vs Right Bind in both frontal and occipital modules during both encoding and

Table 1. Average node gradient over task conditions and participants

FP1	416.44	F8	275.48	T3	188.62	CP3	155.50	P4	247.13
FP2	441.38	FT7	242.58	C3	150.45	CPz	197.48	O1	386.99
F7	295.04	FC3	187.84	Cz	226.38	CP4	197.81	Oz	340.02
F3	224.27	FCz	204.87	C4	207.85	TP8	228.09	O2	349.27
Fz	230.81	FC4	205.10	T4	154.35	P3	220.93	PO1	291.13
F4	224.32	FT8	201.99	TP7	238.02	Pz	249.84	PO2	281.65

**Figure 4.** Example of hierarchical hypothesis tree for hierarchical false discovery rate procedure. 'LiHj' indicates the j th comparison in the i th level of the hierarchy. Red indicates no discovery, green indicates valid discovery, grey indicates exclusion from correction procedure due to false or no discovery made.

maintenance periods. Results found here thus inform on which periods, modules and task related hemisfields are important in Bind tasks. From the paired t -tests, after FDR correction, significant differences were found for the contrast involving Shape vs. Bind conditions in the right hemisfield (left hemisphere stimulation) for both frontal and occipital modules during the encoding period (see Table 2). These showed that the Bind condition weights were greater than those of the corresponding Shape conditions. No differences were found in the maintenance period and, further, no differences were discovered when contrasting Shape vs Bind conditions in the Left hemisfield for either encoding or maintenance periods.

Level 2

In the second level of analysis, we perform MDE over non-overlapping 20ms (5 time samples) windows over the modular weights in Level 1. Due to the dependencies stated in the methods section, our analysis now focuses only on those hypotheses from which their parent hypothesis in the first level were seen as 'true discoveries'. Thus, we present results of the MDE for frontal and occipital modules during the encoding period of Shape vs Bind condition contrasts displayed in the right hemisfield. Further, we study the BMDE of frontal and occipital modules to discover if there may be epochs where dependencies occurring between these regions shows strong effects.

After FDR correction, effects are found in the MDE of the occipital module in the epochs between 100-120ms and 120-140ms. No effects are found in these small windows for the frontal module MDE. The BMDE of occipital and frontal modules shows an effect in the epoch of 120-140ms (see Table 3).

Discussion

We found evidence that the contrasting brain function of Shape vs Bind conditions occurs during the encoding period in both the frontal and occipital modules, which are regions classically associated with task performance and visual attention. This supports the evidence found in Parra et al.²⁷ and Pietto et al.⁷ that these tasks involve rapid functional activity in the frontal module which is picked up by the EEG.

Importantly, we found that this activity was clearly evident in the right hemisfield condition but not so in the left hemisfield

Table 2. *p*-values for paired *t*-tests of modular sum of edge weights in Shape vs. Shape-colour binding conditions. O = occipital module, F = frontal module, E = encoding period, M = maintenance period, L = left hemisfield condition, R = right hemisfield condition. Blue = true discovery, red = false discovery, black = null hypothesis not rejected at the 5% level.

O.E.L	O.M.L	O.E.R	O.M.R	F.E.L	F.M.L	F.E.R	F.M.R
0.1873	0.8709	0.0102	0.4514	0.2119	0.9040	0.0044	0.4806

Table 3. *p*-values for paired *t*-tests of Modular Dirichlet Energy (MDE) and Between MDE (BMDE) in Shape vs. Shape-colour binding conditions. Legend as in Table 2.

Time (ms)	MDE - O.E.R	MDE - F.E.R	BMDE - F.O.E.R
0-20	0.0500	0.1700	0.1009
20-40	0.0491	0.3323	0.1126
40-60	0.0355	0.6190	0.1521
60-80	0.0642	0.3723	0.1952
80-100	0.0353	0.6359	0.0457
100-120	0.0033	0.6722	0.0084
120-140	0.0043	0.1198	0.0033
140-160	0.0825	0.0317	0.0141
160-180	0.2373	0.1099	0.0195
180-200	0.9287	0.6171	0.9644

condition, providing evidence to suggest that there is better sensitivity of EEG activity in tests designed for the right hemisfield. Right hemisfield implies stimulation of the left brain hemisphere which is classically the more task-oriented half of the brain. From this we conjecture that a more direct route, and so less convoluted connectivity, is provided by left brain stimulation for task related activity. It follows that, for the most clinically relevant biomarker for AD by using these tasks in conjunction with the EEG, performance of tasks presented in the right hemisfield may provide more rich information and thus greater sensitivity to impaired activity than those presented elsewhere on the screen.

From the MDE, we note that the effects reported in the occipital module appear to be driven by activity between 100-140ms into the encoding phase of the task. This coincides with the P100 of visual evoked potentials and shows that with our methodology we are able to pick up on event related potential (ERP) activity over the network, which was previously impossible in functional brain network studies because of connectivity values being necessarily computed from information over longer epochs. During P100, then, the Bind condition exhibited stronger MDE in the occipital module than their Shape counterparts, implying greater visual response, and so greater work load, in the Bind condition. This is in accordance with expectations that the Bind condition involve an increased working memory load than the Shape condition. The involvements of visual association cortices in regions of the occipital lobe during short-term memory binding has been documented previously⁶. This appears to be a key area of the visual integrative functions. Recent studies using EEG based methods have confirmed the involvement of these regions in the poor performance found in patients at risk of AD^{7,27}.

Recent electrophysiological studies indicate that frontal nodes may be contributing both specific (i.e. binding) and more general resources during working memory processing. The effect seen here between the frontal and occipital modules from 120-140ms concurs with this, suggesting that a contrast exists in the functional dependency between these regions for Shape vs Bind conditions shortly after the onset of P100 activity. Particularly the network appears more integrated and thus efficient¹⁸ in the shape only condition than in the shape-colour binding condition which again relates to increased load of shape-colour binding, pointing reasonably to an inverse dependency of information load with functional efficiency. This information may inform us on the deficits found in the clinical setting. Alzheimer's disease is characterised by both deficits in new learning (which relates to the encoding period) and rapid forgetting, so that pinpointing spatio-temporal abnormalities in the biological substrates that underpin these deficits is essential both to understand key disease processes and as a step towards defining a useful biomarker of preclinical AD. On this basis, we conjecture that this occipital-frontal dependency is weakened in AD patients. It is reasonable to predict that this effect will be noticeable in future clinical studies and thus could eventually prove useful in providing an indicator for a sensitive biomarker.

The results suggest a focused prolonged functional difference between Shape and Bind conditions beginning in the occipital area at around 100ms, shifting to a dependency between occipital and frontal areas from 120ms to 140ms and even shifting towards the frontal area at 140ms, see Fig. 5. Even though the *p*-value of 0.0317 for the mentioned frontal effect has been rejected by the FDR procedure, the strong chronological dependency of *p*-values over non-overlapping epochs must be taken into account. That is to say, to accept an effect in one epoch but reject as false an effect found in a subsequent epoch, which is

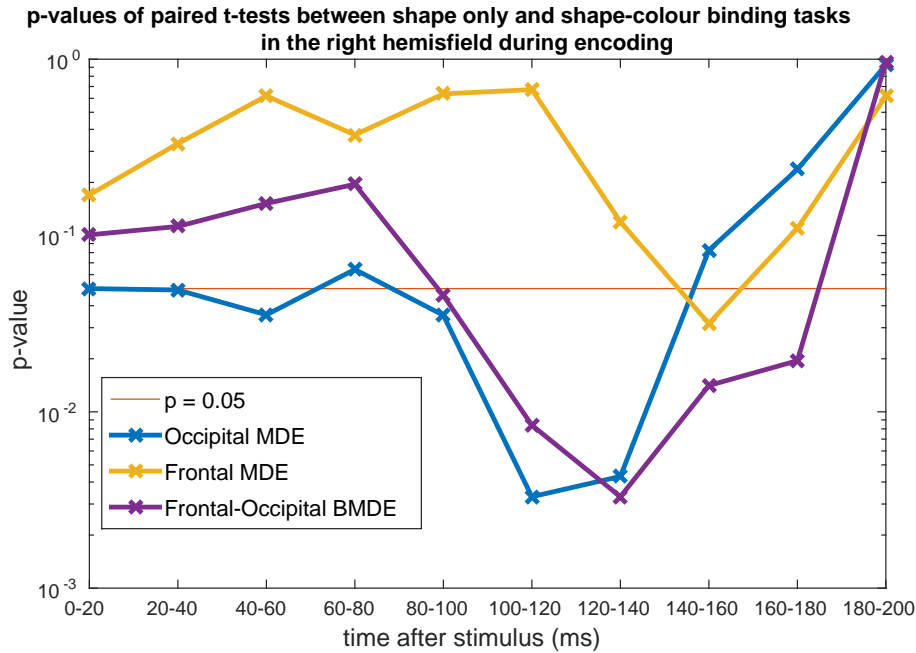


Figure 5. The p -values for shape only vs. shape-colour binding contrasts in the right hemisfield during the encoding period for the Modular Dirichlet Energy (MDE) in the occipital module (blue) and the frontal module (yellow) along side the Betweenness Modular Dirichlet Energy (BMDE) of the occipital and frontal modules calculated over non-overlapping 20ms (5 time sample) windows.

highly chronologically dependent on the former, should require a much stronger justification than if no such dependency existed. Additionally, it is noticeable that all these effects have entirely vanished by the 180-200ms epoch, which is in accordance with the lack of findings found for the maintenance period.

It is important to note that, though no driving effects were accepted as true discoveries in the frontal module using MDE and BMDE, this does not mean that the effect found in the first level was not real, but rather that the effect is perhaps aggregated more over the whole epoch rather than particularly present in any one epoch. Similarly, we do not state that for the rest of the epochs in the occipital module and interactions of occipital and frontal modules there is no effect to be found, but rather that the effects are less concentrated there. Moreover, these results clearly show the importance of high temporal resolution EEG for functional network studies in providing information impossible to obtain in state-of-the-art fMRI research.

In application, the MDE proves to be a sensitive and highly flexible methodology for EEG analysis, both topologically and temporally, providing a unique platform to study EEG activity, such as ERPs, as they apply to functional brain networks. In fact, we showed that not only can MDE pick up on well documented EEG activity, but it can extend our understanding of that activity as a dynamic interdependent activity between different brain areas, progressing our understanding beyond singular channel effects.

Technically, implementation of MDE and its related components could narrow to the level of single time samples, although in practice this would be difficult to justify for EEG recordings. However, as EEG technology improves and knowledge of brain function deepens, as shown here, this method has the potential for pinpointing shifts in functional brain dynamics to the millisecond. As with any such generalisable technique, the flexibility of this methodology means that the potential number of tests which can be carried out is huge. It is important then, as demonstrated here, to make a rigorous set of hypotheses before implementation.

Acknowledgements

KS is funded by the EPSRC. KS was awarded a JM Lessells Travel Scholarship from the Royal Society of Edinburgh to undertake collaborative research at EPFL. NS was supported by SNF grant 200021 154350/1 for the project “Towards signal processing on graphs”. AI is supported by CONICET, CONICYT/FONDECYT Regular (1130920), FONCyT-PICT 2012-0412, FONCyT-PICT 2012-1309, FONDAP 15150012, and INECO Foundation. MAP work was supported by Alzheimer’s Society, Grant # AS-R42303. This study was also supported by the MRC grant # MRC-R42552, awarded to MAP in collaboration with AI and JMS. We thank Jamie Crowther who assisted with data collection. We also acknowledge the support from the Alzheimer’s Scotland Dementia Research and the Centre for Cognitive Ageing and Cognitive Epidemiology part of the cross council Lifelong Health and Wellbeing Initiative (MR/K026992/1) both from the University of Edinburgh.

Author contributions statement

MAP, AI, KS and JE formulated the hypotheses. KS, BR and NS developed the theory of MDE, supervised by PV. KS BR and JE conceived the methodology. MAP and JMS contributed to the discussion. MAP and SR collected the data. KS performed the analysis of the data and wrote the manuscript. All authors reviewed the manuscript.

Additional information

The authors declare no competing financial interests.

References

1. Parra, M.A., Abrahams, S., Logie, R.H., & Della Sala, S., Visual short-term memory binding in Alzheimer’s disease and depression. *J.Neurol.*, **257**(7), 1160-1169. doi:10.1007/s00415-010-5484-9 (2010).
2. Parra, M.A. et al., Visual short-term memory binding deficits in familial Alzheimer’s disease. *Brain*, **133**(9): 2702-2713. doi: 10.1093/brain/awq148 (2010).
3. Parra, M.A., et al., Short-term memory binding deficits in Alzheimer’s disease. *Brain*, **132**(Pt 4): 1057-1066. doi: 10.1093/brain/awp036 (2009).
4. Ibáñez, A., & Parra, M.A., Mapping memory binding onto the connectome’s temporal dynamics: toward a combined biomarker for Alzheimer’s disease. *Frontiers in Human Neuroscience*, **8**(237): doi: 10.3389/fnhum.2014.00237 (2014).
5. Brockmole, J. R., Parra, M. A., Della Sala, S., & Logie, R. H., Do binding deficits account for age-related decline in visual working memory?, *Psychonomic Bulletin and Review*, **15**(3): 543-547 (2008).
6. Parra, M.A., Della Sala, S., Logie, R.H., Morcom, A.M., Neural correlates of shape-color binding in visual working memory. *Neuropsychologia*, **52**(0): 27-36 (2014).
7. Pietto, M., et al., Behavioural and electrophysiological correlates of memory binding deficits in patients at different risk levels for Alzheimer’s disease. *Journal of Alzheimer’s Disease*, (2016, in press).
8. Delbeuck, X., Collette, F., & Van der, L. M., Is Alzheimer’s disease a disconnection syndrome? Evidence from a crossmodal audio-visual illusory experiment. *Neuropsychologia*, **45**(14): 3315-3323 (2007).
9. Delbeuck, X., Van der Linden, M., & Collette, F., Alzheimer’s disease as a disconnection syndrome? *Neuropsychology Review*, **13**(2): 79-92 (2003).
10. Rhodes, S., Parra, M. A., & Logie, R. H., Ageing and feature binding in visual working memory: The role of presentation time. *The Quarterly Journal of Experimental Psychology*, **69**(4): 654-668 (2016).
11. Luria, R., Vogel, E.K., Shape and color conjunction stimuli are represented as bound objects in visual working memory. *Neuropsychologia*, **49**: 1632-1639 (2011).
12. da Silva, F.L., EEG and MEG: Relevance to Neuroscience. *Neuron*, **80**(5): 1112-1128 (2013).
13. Dauwels, J., Vialatte, F.B., & Cichocki, A., On the early diagnosis of Alzheimer’s disease from EEG signals: a mini-review. in Wang, R., & Gu, F., (Eds.), *Advances in cognitive neurodynamics (II)*, Springer Netherlands, 709-716 (2011).
14. Snaedal, J., et al., The use of EEG in Alzheimer’s disease, with and without scopolamine - a pilot study. *Clinical Neurophysiology*, **121**(6): 836-841, doi: 10.1016/j.clinph.2010.01.008 (2010).
15. van Straaten, E.C., Scheltens, P., Gouw, A.A. Stam, C.J., Eyes-closed task-free electroencephalography in clinical trials for Alzheimer’s disease: an emerging method based upon brain dynamics. *Alzheimer’s Research & Therapy*, **6**(9): 86 (2014).

16. Sporns, O., Discovering the human connectome. *MIT Press*, MA, USA (2012).
17. Bassett, D.S., & Bullmore, E., Small-world brain networks. *Neuroscientist*, **12**: 512, doi: 10.1177/1073858406293182 (2006).
18. Bullmore, E., Sporns, O., Complex brain networks: graph theoretical analysis of structural and functional systems. *Nature Reviews*, **10**: 186-198 (2009).
19. Stam, C.J., Modern network science of neurological disorders. *Nature Reviews*, **15**: 683-695 (2014).
20. Brier, M.R. et al., Functional connectivity and graph theory in preclinical Alzheimer's disease. *Neurobiol Aging*, **35**(4): 757-768. doi: 10.1016/j.neurobiolaging.2013.10.081 (2014).
21. Fallani, F.D.V., Richiardi, J., Chavez, M., Achard, S., Graph analysis of functional brain networks: practical issues in translational neuroscience. *Phil. Soc. R. Soc. B*, doi: 10.1098/rstb.2013.0521 (2014).
22. Papo, D., Zanin, M., Pineda-Pardo, J.A., Boccaletti, S., Buldu, J.M., Functional brain networks: great expectations, hard times and the big leap forward. *Phil. Soc. R. Soc. B*, doi: 10.1098/rstb.2013.0525 (2014).
23. Calhoun, V.D., Miller, R., Pearlson, G., Adali, T., The chronnectome: time-varying connectivity networks as the next frontier in fMRI data discovery. *Neuron*, **84**(2): 262-274 (2014).
24. Shuman, D., Narang, S.K., Frossard, P., Ortega, A., Vandergheynst, P., The emerging field of signal processing on graphs. *IEEE Signal Processing Magazine*, **30**(3): 83-98 (2013).
25. Sandryhaila, A., & Moura, J.M.F., Discrete signal processing on graphs. *IEEE Transactions on Signal Processing*, **61**(7): 1644-1656 (2013).
26. Newman, M.E.J., Networks. *Oxford University Press*, Oxford, UK (2010).
27. Parra, M.A. et al., Information sharing within the memory binding network in the prodromal stages of PSEN-1 E280A familial Alzheimer's disease. Submitted (March 2016).
28. Prabhakaran, V., Narayanan, K., Zhao, Z., & Gabrieli, J.D., Integration of diverse information in working memory within the frontal lobe. *Nature Neuroscience*, **3**(1):85-90 (2000).
29. Holme, P., Saramäki, J., Temporal networks. *Physics reports*, **519**(3): 97-125 (2012).
30. Sikdar, S., Ganguly, N., Mukherjee, A., Time series analysis of temporal networks. *Eur. Phys. J. B*, **89**: 11. doi: 10.1140/epjb/e2015-60654-7 (2016).
31. Zimmer, H.D., Visual and spatial working memory: from boxes to networks. *Neurosci. Biobehav. Rev.*, **32**(8): 1373-1395 (2008).
32. Parra, M.A., et al., Memory binding and white matter integrity in familial Alzheimer's disease. *Brain*, **138**(Pt 5): 1355-1369, doi: 10.1093/brain/awv048 (2015).
33. Smith, K., & Escudero, J., A framework for the evaluation of the hierarchical complexity of network topology in EEG functional connectivity. Under revision (May 2016).
34. Yekutieli, D., Hierarchical false discovery rate-controlling methodology. *Journal of the American Statistical Association*, **103**(481): 309-316 (2008).

Supplementary Material: Mathematical Formulation of Modular Dirichlet Energy

Let $G = (\mathcal{V}, \mathbf{f}, \mathcal{E}, \mathbf{W})$ be the mathematical representation of an undirected, labeled graph where $\mathcal{V} = \{1, \dots, n\}$ is the vertex set, or labels, of the graph, $\mathbf{f} = \{f_1, f_2, \dots, f_n\}$ is the graph signal, or vertex amplitudes, indexed by \mathcal{V} , $\mathcal{E} = \{(i, j) \text{ s.t. } i \text{ is adjacent to } j \text{ for } i, j \in \mathcal{V}\}$ is the edge set with $|\mathcal{E}| = 2m$ and

$$\mathbf{W} = \begin{cases} w_{ij} & (i, j) \in \mathcal{E} \\ 0 & \text{otherwise} \end{cases}$$

is the positive weighted adjacency matrix of edge weights indexed by \mathcal{E} , where w_{ij} is a measure of strength of relationship between nodes i and j . Then we call $(\mathcal{V}, \mathbf{f})$ the vertex space of the graph and $(\mathcal{E}, \mathbf{W})$ the edge space of the graph so that G is a dual space composed of the vertex and edge spaces where every element of the edge set in the edge space is an ordered pair of elements from the vertex set in the vertex space.

An illustration of a graph with a graph signal is shown in Fig. 6. The blue circles represent the nodes of the network and the lines connecting them represent the edges. The graph signal is composed of the node amplitudes which are represented in Fig. 6 by the orange and blue lines- positive and negative values, respectively.

Modularity

We define a subgraph, \mathcal{S}_x , of G as $\mathcal{S}_x = (\mathcal{V}_x, \mathbf{f}_x, \mathcal{E}_x, \mathbf{W}_x)$ such that $\mathcal{V}_x \subset \mathcal{V}$ and $\mathcal{E}_x \subset \mathcal{E}$ where elements of \mathcal{E}_x are ordered pairs of elements in \mathcal{V}_x , \mathbf{f}_x is the graph signal indexed by \mathcal{V}_x and \mathbf{W}_x is the weighted adjacency matrix indexed by \mathcal{E}_x . Further we define a full subgraph, G_x , of G as a subgraph such that $\mathcal{E}_x = \{(i, j) \in \mathcal{E} \text{ s.t. } i, j \in \mathcal{V}_x\}$. That is, all of the edges that exist between vertices of the graph which lie in the subset, \mathcal{V}_x , are exactly those that exist in the full subgraph, G_x .

We now define a module, for some vertex subset, \mathcal{V}_x , as the subgraph $\mathcal{G}_x = (\mathcal{V}, \mathbf{f}, \mathcal{H}_x, \mathbf{W}_x)$ of G , where $\mathcal{H}_x = \{(i, j) \in \mathcal{E} \text{ s.t. } i \in \mathcal{V}_x \& j \in \mathcal{V}\} \subset \mathcal{E}$. This contains the full subgraph of \mathcal{V}_x , but also all of the edges for which one of its adjacent vertices is in \mathcal{V}_x but the other exists in $\mathcal{V} \setminus \mathcal{V}_x$.

Now, modularity is concerned with disjoint partitions of a graph by the vertex set. Particularly, from the above definitions, we can decompose a graph into disjoint modules corresponding to a disjoint decomposition of the vertex set $\mathcal{V} = \bigsqcup_{x=1}^M \mathcal{V}_x$ such that

$$G = \bigcup_{x=1}^M \mathcal{G}_x = \bigcup_{x=1}^M (\mathcal{V}_x, \mathbf{f}_x, \mathcal{H}_x, \mathbf{W}_x).$$

In fact, $\{\mathcal{H}_x\}_{x=1}^M$ are mutually disjoint subsets because (i, j) and (j, i) , although referring to the same undirected edge in the graph, are separate elements of the edge set \mathcal{E} and appear in separate modules given that i and j are in different subsets of \mathcal{V} . Given this property it is useful now to define a set operation we name the edge intersection, \wedge , such that

$$\mathcal{H}_x \wedge \mathcal{H}_y = \{(i, j) \in \mathcal{E} \text{ s.t. } i \in \mathcal{V}_x \& j \in \mathcal{V}_y \text{ or } j \in \mathcal{V}_x \& i \in \mathcal{V}_y\},$$

$$\mathbf{W}_x \wedge \mathbf{W}_y = \begin{cases} w_{ij} & \text{if } (i, j) \in \mathcal{E} \text{ and either } i \in \mathcal{V}_x \& j \in \mathcal{V}_y \\ & \text{or } j \in \mathcal{V}_x \& i \in \mathcal{V}_y \\ 0 & \text{otherwise} \end{cases}$$

and, for two subgraphs, \mathcal{S}_x and \mathcal{S}_y , of G ,

$$\mathcal{S}_x \wedge \mathcal{S}_y = (\mathcal{V}_x \cup \mathcal{V}_y, \mathbf{f}_x \cup \mathbf{f}_y, \mathcal{H}_x \wedge \mathcal{H}_y, \mathbf{W}_x \wedge \mathbf{W}_y).$$

Modular Dirichlet Energy

The Dirichlet energy of the graph G is defined as

$$E(G) = \sum_{i,j=1}^n w_{ij}(f_i - f_j)^2, \quad (6)$$

which is an inverse measure of the smoothness of the graph signal \mathbf{f} over G^{24} . Particularly, the node gradient at node i is an important measure of the smoothness of the graph signal at node i and is defined as

$$E(i) = \sum_j w_{ij}(f_i - f_j)^2. \quad (7)$$

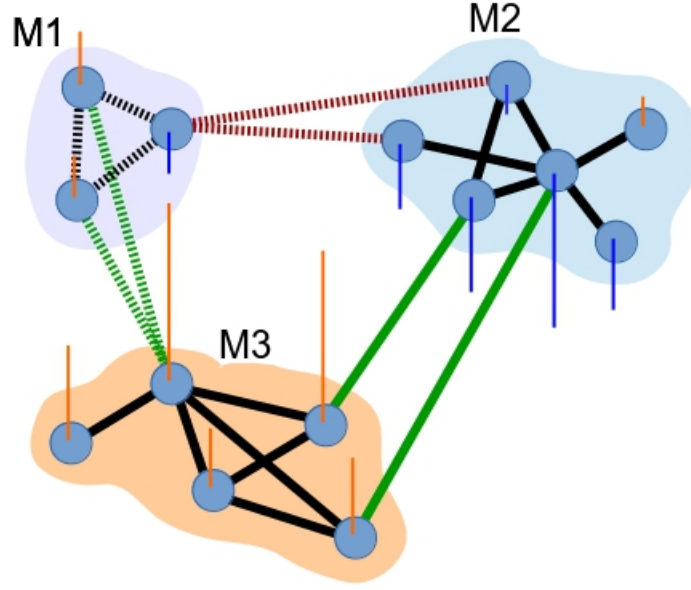


Figure 6. Illustration of a graph with a graph signal, indicated by the orange (positive) and blue (negative) lines at the nodes, decomposed into modules M1, M2 and M3. The dashed lines indicate all the edges associated with module M1.

Note that the elements in the sum of (6) have a one to one mapping to the edge set, \mathcal{E} , of G . It follows that there is a natural decomposition of the Dirichlet energy in (6), corresponding to any disjoint composition of the underlying graph into modules, such that

$$E(G) = \sum_{x=1}^M \sum_{i \in \mathcal{V}_x} \sum_{j \in \mathcal{V}} w_{ij} (f_i - f_j)^2,$$

and we define the Modular Dirichlet Energy (MDE) of \mathcal{G}_x to be

$$MDE(\mathcal{G}_x) = \sum_{i \in \mathcal{V}_x} \sum_{j \in \mathcal{V}} w_{ij} (f_i - f_j)^2. \quad (8)$$

$$= \sum_{i, j \in \mathcal{V}_x} w_{ij} (f_i - f_j)^2 + \sum_{p \in \mathcal{V}_x} \sum_{q \in \mathcal{V} \setminus \mathcal{V}_x} w_{pq} (f_p - f_q)^2, \quad (9)$$

so that the sum of MDEs equals the total Dirichlet energy in the graph (8), satisfying energy preservation, and the MDE accounts both for the Dirichlet energy within the module and the Dirichlet energy of the module interacting with the rest of the graph (9), which directly corresponds to modules in networks. The dashed lines in Fig. 6 represent all the edges, and corresponding Dirichlet energy components, of the module M1. Further, we can define the within module Dirichlet energy and between module Dirichlet energy (BMDE) as

$$E(G_x) = \sum_{i, j \in \mathcal{V}_x} w_{ij} (f_i - f_j)^2, \quad (10)$$

and, for two disjoint modules \mathcal{G}_x and \mathcal{G}_y ,

$$BMDE(\mathcal{G}_x, \mathcal{G}_y) = \sum_{i \in \mathcal{V}_x} \sum_{j \in \mathcal{V}_y} w_{ij} (f_i - f_j)^2, \quad (11)$$

respectively. In Fig. 6, the black lines represent within module edges and energy components of each module and the dashed brown lines indicate the between module edges and energy components of modules M1 and M2. Now,

$$MDE(\mathcal{G}_x) = E(G_x) + \sum_{y \neq x} BMDE(\mathcal{G}_x \wedge \mathcal{G}_y), \quad (12)$$

and

$$E(G) = \sum_{x=1}^M \left(E(G_x) + \sum_{y \neq x} BMDE(\mathcal{G}_x \cap \mathcal{G}_y) \right). \quad (13)$$

That is, the MDE at module \mathcal{G}_x of G is the within module Dirichlet energy, or Dirichlet energy of the subgraph, G_x , combined with the sum of the between module Dirichlet energies from \mathcal{G}_x to all other modules in the graph (12), which we call the Modular Interaction Dirichlet Energy (MIDE), i.e.

$$MIDE(\mathcal{G}_x) = \sum_{y \neq x} BMDE(\mathcal{G}_x \cap \mathcal{G}_y). \quad (14)$$

The green lines of Fig. 6 represent the interaction edges and energy components of module M2. Further, the total Dirichlet energy of G is the sum of all within module Dirichlet energies and BMDEs (13). Note that the elements in $(\mathcal{V}_x, \mathcal{H}_x) \wedge (\mathcal{V}_y, \mathcal{H}_y)$ corresponds exactly to those elements in the sum of (11).

For graph signals which also have a temporal dimension, i.e. $\mathbf{F} = [\mathbf{f}^0, \mathbf{f}^1, \dots, \mathbf{f}^Y]$, an $n \times Y$ matrix of chronologically ordered graph signals $\mathbf{f}^i = \{f_1^i, f_2^i, \dots, f_n^i\}$, the Dirichlet energy of the signal during time period $[t_0, t]$ is just the sum of the individual Dirichlet energies at each point in time:

$$E(G)|_{[t_0, t]} = \sum_{s=t_0}^t \sum_{i,j=1}^n w_{ij} (f_i^s - f_j^s)^2.$$

Thanks to linearity, this extends straightforwardly to all definitions above. By looking at short intervals of graph signals, $[t_0, t]$, we can study moments in time of the network behaviour by looking at the graph signal in the short interval acting over the graph defined by connectivity of the whole epoch and thus probe the connectivity information for dynamic behaviour within the epoch on which the graphs are constructed.

Computation of Modular Dirichlet Energy

It is known that for a graph, G , with Laplacian, $\mathbf{L} \in \mathbb{R}^{n \times n}$ and signal $\mathbf{F} \in \mathbb{R}^{n \times Y}$, the Dirichlet energy is $E(G) = 2\text{tr}(\mathbf{F}^T \mathbf{L} \mathbf{F})$ ²⁴, where $\text{tr}()$ is the trace function for matrices. Note, the multiplication by 2 comes from the fact that w_{ij} and w_{ji} relate to edges (i, j) and (j, i) which are regarded as separate elements. This then corresponds with the theoretical formulation of a graph, although, in fact, they are always equal in an undirected graph and relate to the same undirected edge. Now, the within module Dirichlet energy of module \mathcal{G}_x is just

$$E(G_x) = 2\text{tr}(\mathbf{F}_x^T \mathbf{L}_x \mathbf{F}_x),$$

where \mathbf{L}_x is the Laplacian of full subgraph G_x and \mathbf{F}_x is the subset of \mathbf{F} corresponding to the vertex subset \mathcal{V}_x .

To compute $E(\mathcal{G}_x)$ easily, we wish to express it also in terms of operations on the Laplacian. We can do this straightforwardly using basic set theoretic relationships on the underlying graph because the elements $\{w_{ij}(f_i - f_j)^2\}_{(i,j) \in \mathcal{E}}$ constitute a set with a one to one mapping to the edge set, \mathcal{E} . Let $A = E(G_x)$, $B = E(G_{\setminus x})$ and $2C = E(\mathcal{G}_x \wedge \mathcal{G}_y)$, where $G_{\setminus x}$ is the full subgraph whose vertex set is the complement \mathcal{V}_x and we choose $2C$ because (i, j) and (j, i) are treated as separate elements both with corresponding elements in $E(\mathcal{G}_x \wedge \mathcal{G}_y)$. Then we know how to compute A , B and $A + B + 2C = E(G)$ and we find $E(\mathcal{G}_x)$ as

$$\begin{aligned} MDE(\mathcal{G}_x) &= A + C \\ &= A + \frac{1}{2}((A + B + 2C) - A - B) \\ &= \frac{1}{2}(A + (A + B + 2C) - B) \\ &= \frac{1}{2}(E(G_x) + E(G) - E(G_{\setminus x})) \\ &= \text{tr}(\mathbf{F}_x^T \mathbf{L}_x \mathbf{F}_x + \mathbf{F}^T \mathbf{L} \mathbf{F} - \mathbf{F}_{\setminus x}^T \mathbf{L}_{\setminus x} \mathbf{F}_{\setminus x}), \end{aligned}$$

Following from this, it is straightforward to see that the MIDE of a module can be expressed as

$$\begin{aligned} MIDE(\mathcal{G}_x) &= MDE(\mathcal{G}_x) - E(G_x) \\ &= MDE(\mathcal{G}_x) - 2\text{tr}(\mathbf{F}_x^T \mathbf{L}_x \mathbf{F}_x) \\ &= \text{tr}(\mathbf{F}^T \mathbf{L} \mathbf{F} - \mathbf{F}_x^T \mathbf{L}_x \mathbf{F}_x - \mathbf{F}_{\setminus x}^T \mathbf{L}_{\setminus x} \mathbf{F}_{\setminus x}), \end{aligned} \quad (15)$$

where (15) comes from (12). Finally, taking $\mathcal{G}_x \cup \mathcal{G}_y = (\mathcal{V}_x \cup \mathcal{V}_y, \mathbf{F}_x \cup \mathbf{F}_y, \mathcal{H}_x \cup \mathcal{H}_y, \mathbf{W}_x \cup \mathbf{W}_y)$ to be the module of the union of modules \mathcal{G}_x and \mathcal{G}_y , the between module dirichlet energy of \mathcal{G}_x and \mathcal{G}_y is

$$BMDE(\mathcal{G}_x, \mathcal{G}_y) = \text{tr}((\mathbf{F}_x \cup \mathbf{F}_y)^T \mathbf{L}_{x \cup y} (\mathbf{F}_x \cup \mathbf{F}_y) - \mathbf{F}_x^T \mathbf{L}_x \mathbf{F}_x - \mathbf{F}_y^T \mathbf{L}_y \mathbf{F}_y).$$